Push-out behaviour of demountable injected vs. blind-bolted connectors in FRP decks

Csillag, Fruzsina; Pavlovic, Marko

DOI
10.1016/j.compstruct.2021.114043

Publication date
2021

Document Version
Final published version

Published in
Composite Structures

Composite Structures 270 (2021) 114043

Contents lists available at ScienceDirect

Composite Structures

journal homepage: www.elsevier.com/locate/compstruct

Push-out behaviour of demountable injected vs. blind-bolted connectors in FRP decks

Fruzsina Csillag [a], Marko Pavlović [b,*]

[a] Arup, Naritaweg 118, 1043 CA Amsterdam, the Netherlands
[b] Delft University of Technology, Stevinweg 1, 2628CN Delft, the Netherlands

ARTICLE INFO

Keywords:
FRP
Push-out tests
Shear connectors
steel-FRP hybrid structure
Blind bolts
Injected steel-reinforced resin
nonlinear FEA
Damage modelling
Explicit analysis
Hashin damage model

ABSTRACT

The main challenge for realizing competitive hybrid steel-FRP structures, such as bridges, carparks, is to make the steel and FRP components work together. In this study shear resistance, stiffness and ductility of three types of demountable bolted shear connectors are examined. Two blind-bolted M20 shear connectors and a novel, injected steel-reinforced resin (SRR) connection are selected to perform push-out experiments in web-core FRP decks. Failure modes of excessive bearing in FRP and bolt shear failure for blind-bolted and injected connectors, respectively, are identified. Nonlinear, highly detailed finite element (FE) models were also built and validated by results of the push-out tests to provide insights to the load-transfer mechanism. Analysis of internal forces and deformation through FE results reveals that blind bolted shear connectors provide high shear resistance and slip capacity thanks to the shear sleeves and catenary effects. The injected SRR connector shows distinct and centric load transfer owing to gapless design.

1. Introduction

Hybrid bridges composed of FRP deck elements fastened or adhesively joined to the primary steel girders can be a competitive solution to reduce maintenance costs of bridge infrastructure. FRP decks can be used for steel-FRP hybrid structural systems in newly built construction and/or to extend lifetime of existing bridges. FRP is known for its excellent fatigue performance, for example in wind turbine blades or airplanes, and therefore offers the potential to solve fatigue problems of existing steel decks. By placing the durable FRP deck on top of steel superstructure (cross and/or main bridge girders), much better resistance to degradation due to water and de-icing salts can be achieved compared to the existing hybrid solutions using concrete decks.

Steel-FRP bridges can be designed by either exploiting or neglecting hybrid interaction between the FRP deck and steel girders. Due to lack of knowledge on interaction and sound solutions for shear connection between FRP deck and steel structure, several pioneering examples of traffic steel-FRP bridges are designed conservatively by excluding hybrid interaction [1–3]. Employing hybrid interaction can increase bending stiffness of the longitudinal girders. Knippers and Gabler [4] designed the first major FRP-steel hybrid highway bridge, the Friedberg bridge in Germany. Making use of the hybrid interaction with adhesive bonding between the main structural components helped to reduce the vertical displacement of the 21.5 m span hybrid bridge by 20% compared to steel stringers alone. More importantly using a shear connection with practically no or very little slip can prevent repetitive relative movement between the deck and the girders. For example, allowing constant slip between the FRP deck and steel girders due to traffic load on bridges can result in wear of materials and therefore unpredictable fatigue behaviour of the connection detail. Hybrid interaction on the other hand will lead to unwanted internal stresses due to readily higher thermal expansion coefficient of the FRP deck vs. steel girders which is the motivation to use slip connectors with slotted holes in most of up-to-date applications. Regardless providing the hybrid interaction or not, the key for successful application of FRP decks in such bridges lies in predictable and reliable connection details.

Two main types of shear connector systems exist in steel-FRP hybrid bridges: connection with mechanical fasteners (shear studs, dowels, bolts, steel clamps) and adhesive bonding. Moon et al.[5] examined a grouted shear stud type connection for pultruded decks, incorporating steel spirals around each shear stud for stronger confinement of the grout. The connection performed well in both static and fatigue push-out tests and it was shown that the larger volume of grout reduces stress concentrations behind the shear studs and mitigates

* Corresponding author.
E-mail addresses: Fruzsina.Csillag@arup.com (F. Csillag), m.pavlovic@tudelft.nl (M. Pavlović).

https://doi.org/10.1016/j.compstruct.2021.114043
Received 25 October 2020; Revised 30 March 2021; Accepted 29 April 2021
Available online 4 May 2021

local crushing of the bottom face laminate. Chou and Chen [6] found shear resistance of nearly 110 kN and 10 mm slip before failure of 16 mm diameter welded headed studs embedded in cement based grout within FRP deck. Davalos et al. developed, and Righman et al. [1] further studied a sleeve-type shear connector. The static tests showed an average ultimate load of 136 kN per stud, governed by delamination of the FRP and fracture of the shear studs.

Satasivan and Bai [7] conducted 4-point bending experiments on $L = 2.7$ m span steel beams with GFRP deck composed of box profiles and pultruded plates. Hybrid beams with unidirectional and bidirectional orientation of the deck resulted in approximately 40% and 90% greater maximum bending resistance than that of the reference steel beam, respectively. Keller and Gürtler [8] performed 4-point bending tests on 10 m long steel-FRP hybrid beams with two types of adhesively bonded pultruded decks (DuraSpan and ASSET). Full hybrid interaction, up to failure, between the top steel flange and lower FRP deck face panels was accomplished. Hybrid interaction enabled the increase of failure load by 52% and 56% for ASSET girders and DuraSpan girders respectively, while the deflections at serviceability limit state (SLS) reduced by 50% in case of ASSET deck, and 23% in case of DuraSpan deck compared to the reference steel beam.

The conclusion from all researches is that, the degree of hybrid interaction between FRP deck and steel girder depends on two parameters: the stiffness properties of the shear connectors, and the in-plane deck stiffness in the longitudinal direction of the bridge axis. Adhesive bonding gives good results but greater application in practice is hindered by lack of: quality control, unified and predictable bonding properties, demountability and also by the presence of large stress concentrations and brittle failure modes. On the other hand, as was demonstrated, only limited knowledge is available on the performance of demountable shear connectors in steel-FRP hybrid construction. In the limited examples of bolted connection mentioned above [9,10], relatively low degree of hybrid interaction was obtained.

The aim of this paper is to investigate the mechanical and functional performance and shear resistance of demountable bolted connectors for FRP decks. The parameter of connector type is varied: two commercially available blind-bolted alternatives and one demountable shear connector system recently developed at TU Delft, utilizing reinforced resin injection and embedded bolt. In total, 10 push-out experiments were carried out according to Eurocode 4 [12]. The failure modes of connectors subjected to shear load are described through analysis of damage patterns and the obtained load-slip curves are evaluated against the connector stiffness, resistance and ductility. Failure modes and in-depth analysis of local load transfer are further analysed through advanced finite element analysis with damage models of FRP, steel and reinforced resin materials. The aim is to improve understanding of failure mechanisms which will build up confidence for usage of such connectors in engineering practice and their further optimization.

2. Investigated demountable connectors

The shear behaviour of two blind bolted shear connectors and a hybrid steel-reinforced resin (SRR) connection technology is evaluated in this research. The illustration of the three shear connector systems is shown in Fig. 1. The main advantage of blind bolts over conventional bolting technology, is that they require only one face access. Therefore, the top surface of the deck can remain intact to maintain good durability against cracks due to running wheels. The drawback is that they need to be installed from underneath the bridge deck mainly through on-site drilled holes through the top flange of the steel girder and the bottom of the FRP deck due to small execution tolerances of approx. 1–2 mm. The Ajax [13] and Lindapter Hollo-Bolt [14] were previously demonstrated as competitive alternatives of headed studs in steel–concrete composite beams in the work of Pathirana [15] and Mirza [16]. However, to the author's best knowledge, no research data has been published on these connectors in steel-FRP composite systems.

The novel, hybrid connection – referred to as 'Injected SRR connection' or abbreviated iSRR hereinafter – consists of a mechanical connector preinstalled on steel flange and embedded inside a cylindrical hole of the FRP panel, see Fig. 1c. In this research, a coupler connector with anchoring bolt inside the panel and the assembly bolt and washer on the outside (steel-flange side) are used to create a demountable connection favourable for reuse in the second lifetime. The goal is to limit damage to the replaceable component, the assembly bolt, while the FRP structure and SRR injection piece should remain intact to allow for reuse. Modification in type of the mechanical connector is possible, such as single or double nut bolted connector used in concrete decks by Pavlovic [17], as well as using the traditional welded headed stud in case demountability is not desired. The mechanical connector is surrounded by steel-reinforced resin (SRR) material, which fills up the socket in the FRP panel by injection after the deck is placed on top of the steel girder. The injection is performed through small holes from the top of the deck which eases execution. Relatively large holes, 60 mm in this research, in the bottom facing of the FRP panel offers tolerance for execution even up to 20 mm per connector, therefore allowing for prefabrication, rather than on-site drilling. Another purpose of the large hole is to reduce the bearing stress peaks (concentrations) due to shear load transfer in the FRP deck.

The injection material, SRR, is composed of a skeleton of steel particles (steel spheres of a few mm diameter) and a polymer resin. The innovation of the SRR material was pioneered by Nijgh [18] in the field of bolted connections in steel structures. According to initial study of [19] steel reinforcement offers 1.5–2 times increased stiffness and reduces creep by roughly 40% compared to pure polymer resin. This is important for application of injection material in a relatively big volume, as in injected SRR connector. However, the strength of the SRR is lower, than that of the pure resin due to the existence of micro cracks at the interfaces between the resin and the steel spheres.

3. Push-out experiments

3.1. Test set-up and specimens

The specimens consisted of two vacuum infused FRP deck panels with integrated webs (web-core panels), a HEB260 (S355) steel profile and 4 shear connectors as can be seen in Fig. 2. There is no specific test guidance for push-out tests on shear connectors in steel-FRP hybrid structures. Therefore initially the recommendations of Annex B of EC4 [12] for steel–concrete structures were followed. This traditional set-up with 8 connectors was initially tested on the first series of Ajax bolt. Unfortunately using 8 connectors resulted in irrelevant failure mode of the FRP panel, because the resistance of the connectors was way too high relative to that of the FRP panels. The irrelevant failure mode of the initial series of Ajax bolt and the force-slip behaviour is shown in Fig. 3b and c, respectively. All further tests were continued with improved set-up (see Fig. 3a) using 4 shear connectors, where desired failure modes of the connectors were obtained.

The InfraCore Inside deck panels fabricated by FiberCore [20] are built-up from Z-layers of GFRP laminates surrounding a PU foam core. The size of the panels was 500x370 mm with a deck thickness of 150 mm. The facings of the deck were 19 mm thick, the transverse webs had a thickness of 8 mm, spaced at 110 mm. The principle fibre direction in the facings (same as the web orientation) was perpendicular to the orientation of steel beam.

In all three groups of specimens, M20 bolts of grade 8.8 were used. In case of Ajax connectors, 26 mm high, 29 mm outer diameter sleeves were used to prevent the threaded part of the bolt getting in contact with the FRP laminate. Lindapter connectors consisted of hexagonal

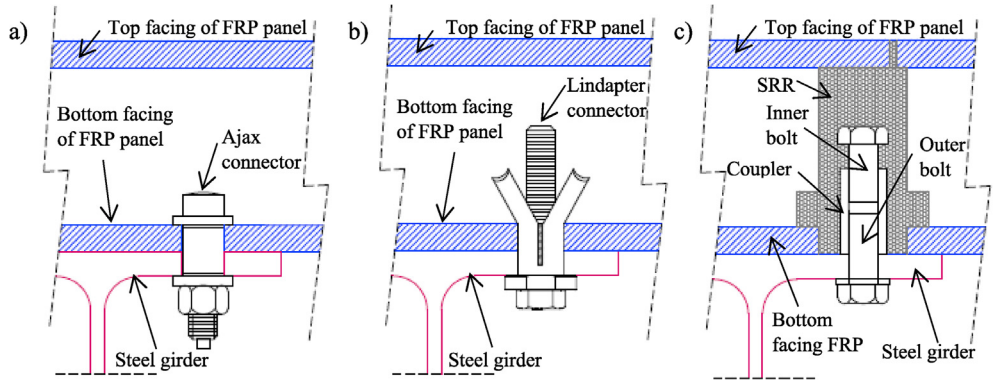

Fig. 1. The selected shear connector systems: a) Ajax, b) Lindapter Hollo-Bolt, c) injected SRR connector.

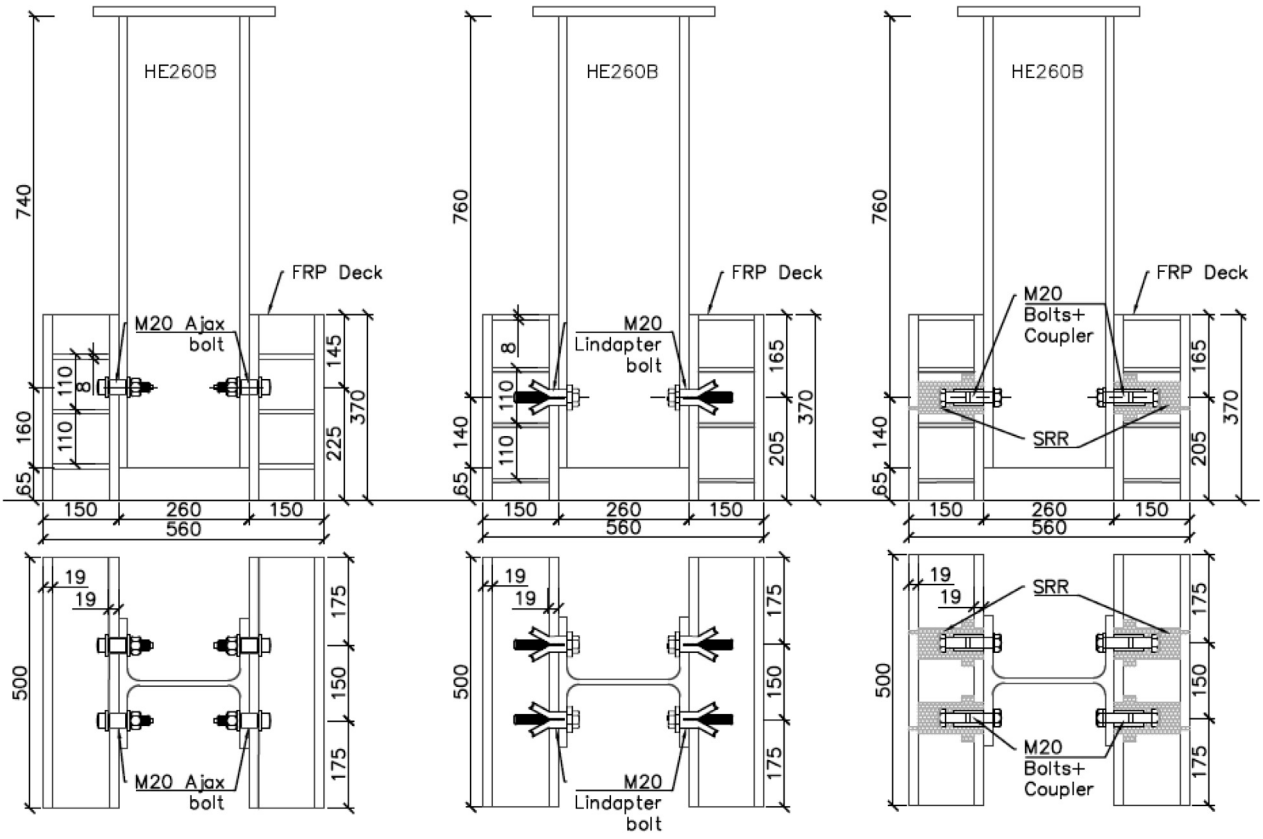

Fig. 2. Push-out specimens: Ajax, Lindapter, injected SRR connectors.

headed M20 × 120 mm bolts with a sleeve of 32.7 mm outer diameter. In the injected SRR connection the M20 coupler had a grade of 10.9 ensuring that the damage will occur in the replaceable outer bolt, not in the coupler itself.

The bolt holes in steel and FRP were sized with 1–2 mm clearance based on the specification of the producers in case of the blind bolts. For the injected SRR connection, 1 mm clearance in steel flange was employed to facilitate bolt installation. The preparation of the blind bolted specimens followed the standard process given by the producers [13,14], although an adjustment had to be made in case of the Ajax specimen: a continuous hole was drilled through the FRP panel to enable installation process due to the long installation tool. For installation of Ajax and injected SRR connection a relatively small amount of torque (60 Nm) was applied. Such torque was enough to cease any clearances but small enough to prevent friction-based load transfer mechanism which was not within the scope of this research. Lindapter connectors required larger torque in order to be installed (fixed) by opening of the sleeve. Torque of 220 Nm was applied instead of 300 Nm specified by the producer. This value was determined in series of lab tests to be large enough to open the sleeve and provide tight contact between the plates but not too high to crash the FRP laminate. The overview of the specimens with the corresponding shear area and hole sizes is given in Table 1. Note that in case of Ajax and Lindapter connectors, in addition to cross section area of the bolt at the threaded part, the shear area includes the cross sectional area of the sleeves which contribute in the shear load transfer at steel-FRP interface.

The vertical space between the bolt and the bottom support varies slightly throughout the specimens (see Fig. 2). This was due to the

a) Final improved set-up with 4 shear connectors b) Traditional (initial) push-out set-up with 8 shear connectors

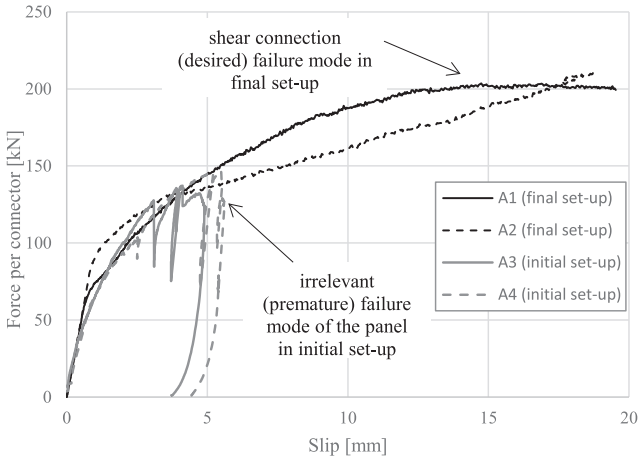

c) Force-slip behaviour in traditional (initial) vs, final push-out set-up

Fig. 3. Push-out test set-up.

Table 1
Overview of the push-out specimens.

Specimen	Shear connector	Shear area of the connector (* including sleeve)	Bolt hole in HEB flange	Bolt hole in FRP
A1, A2	Ajax bolt	582 mm^2 *	30 mm	32 mm
L1, L2, L3	Lindapter Hollo-Bolt	739 mm^2 *	34 mm	35 mm
I1, I2, I3	injected SRR connector	245 mm^2	21 mm	62 mm

imperfection in the production of the panels. In a side sensitivity FE study it was confirmed that the small variance of bolt edge distance does not affect the results.

3.2. Material properties

FRP deck panel with integrated webs is formed in vacuum infusion process using 600 g/m^2 uni-directional and 1200 g/m^2 bi-directional fabrics of E-glass fibre reinforcement embedded in a polyester resin. The result is a multidirectional, anisotropic laminate in the facings (0°/62.5%; 90°/12.5%; ±45°/25%) with fibre volume fraction of V_f = 52% and quasi-isotropic laminate in the webs (V_f = 28%). Material properties of the laminate of the facing, as provided by the producer, are as follows: elastic modulus in principal and perpendicular direction of the laminate, E_1 = 29.2 GPa, and E_2 = 16.8 GPa, respectively; shear modulus G_{12} = 6 GPa; Poisson's ratio ν_{12} = 0.338; density ρ = 1873 kg/m^3.

In the present work, experimental results of double-lap shear tests [21] on FRP plates cut from the facings of the deck panels were used to obtain the pin-bearing strength of the FRP material. The first peak of the load–displacement curve was identified as the pin-bearing strength of 247 MPa see [21] according to ASTM D 5961-05 [22].

In the present application the SRR is in a semi-confined condition, because the surrounding FRP plate provides only relatively flexible support, whereas the PU foam gives almost no resistance against the lateral deformation of the SRR cylinder. Compression and tensile split-

ting tests were performed on SRR cylinders of 62 mm in diameter and 130 mm height, 3 specimens each, in unconfined condition. The mean values of mechanical properties of SRR were determined as: compressive strength of 74.3 MPa; elastic modulus of 9.3 GPa and tensile splitting strength of 10.1 MPa.

3.3. Measurements and loading regime

The specimens were loaded by a hydraulic jack at the top, through a spherical bearing and a thick steel plate ensuring uniform load introduction to the HEB profile. The FRP panels are provided with lateral boundary condition at the bottom by means of hollow profiles connected by two threaded steel rods (Fig. 3) to prevent splitting (delamination) of the FRP panel at the support. Axial force of in the rods up to 50kN was measured and successfully validated by lateral reaction force of lateral boundary conditions in the FE model.

6 LVDTs (Linear Variable Displacement Transducer) were mounted on the specimens: 4 in direction of the load next to the connectors to measure the slip between the steel beam and the FRP deck, and 2 perpendicular to load direction on the front side of the specimen to measure separation of the panels from the steel beam. Distance between the measurement points on the steel flange and the FPR panel, shown as MP1 and MP2 in detail of Fig. 3 respectively, was 50 mm as minimum distance to allow operation of the LVDT. The averaged data from the 4 LVDTs next to connectors was used to produce the load-slip curves of the specimens. The loading regime for standard push-out tests [12] starts with load controlled cycles in the load range of 5% and 40% of the estimated ultimate resistance in order to accommodate settling of the connectors in the holes and eliminate traces of possible sticking friction. Ultimate resistance of the connectors in range of 150–250 kN has been estimated by preliminary FE models and hand calculation. After 26 cycles, the structure is gradually loaded, 2 mm/min, till failure in displacement-controlled mode.

4. Results of push-out experiments

4.1. Failure mode of the Ajax shear connector

Local crushing of the laminate in combination with yielding of the bolts occurred for the Ajax connectors. Excessive damage could be observed in the FRP, involving bearing failure and extended region of delamination failure. Fig. 4 shows the deformed shape of the bolts and the damaged region of the laminate, after the test was completed. It was possible to dismantle the bolts despite the considerable plastic bending deformation they have undergone, thus this system proved to be demountable.

4.2. Failure mode of the Lindapter shear connector

Similarly to the Ajax shear connector, bearing damage of FRP and connector yielding caused the failure of all Lindapter specimens. Due to the same failure mechanism and similar deformation that the specimens have endured, the damaged zone in the FRP panels of Lindapter specimens are comparable in size to those of the Ajax specimens (see Fig. 5). The conical sleeves and the bolt deformed plastically to a great extent at the interface between the FRP and steel plate, see Fig. 5a. In this case, the bolts could not be dismantled, they were sawed in order to disassemble the specimens, hence the criteria for demountability is not met.

4.3. Failure mode of the injected SRR shear connector

Specimens with injected SRR shear connectors failed by the distinct bolt shear failure, see Fig. 6a and d. The bolts could be successfully dismantled from the locations where only the stiffness of the connection was degraded due to damage in iSRR but bolt rupture did not occur (the opposite side of push-out specimen I2), see Fig. 6c. Only negligible damage could be observed around the holes in the FRP panels, which proves the potential of this system to provide reuse of structural components in second lifetime. Specimen I1 showed failure of the injected SRR piece (Fig. 6b), which is attributed to reduced SRR material properties caused by partially faulty injection.

4.4. Force-slip behaviour

The resulting force-slip curves from push-out tests of the specimens with Ajax, Lindapter and injected SRR connectors are shown in Fig. 7. The total force acting on the specimen versus the relative displacement (slip) calculated as an average value of the 4 LVDTs are displayed.

Table 2 summarises the test results, where F_{ult} is the shear resistance per shear connector, the total slip $\delta_{u,tot}$ is decomposed to initial slip δ_{init} accumulated during initial short 25 cycles of loading up to

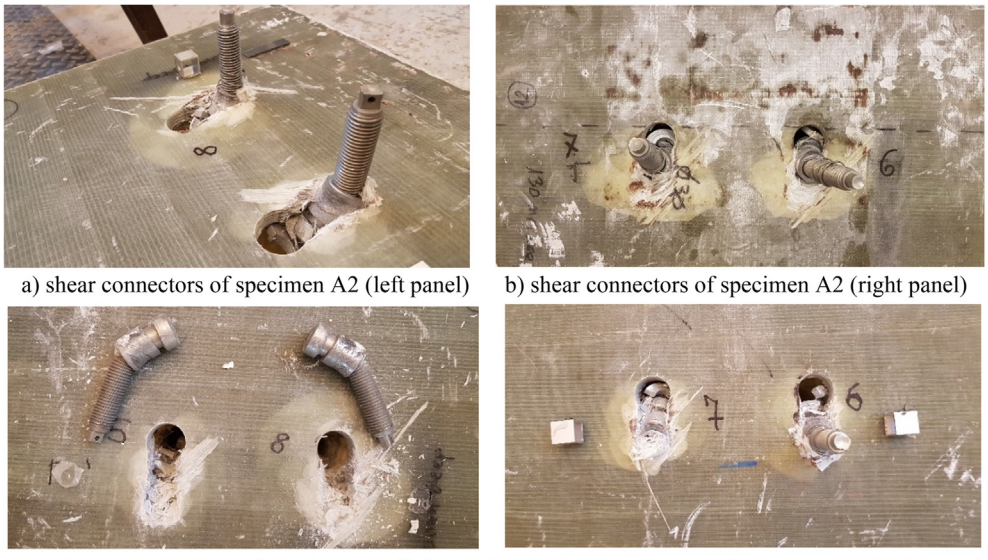

a) shear connectors of specimen A2 (left panel) b) shear connectors of specimen A2 (right panel)

c) shear connectors of specimen A1 (left panel) d) shear connectors of specimen A1 (right panel)

Fig. 4. Deformation of shear connectors and damages of FRP in Ajax push-out specimens.

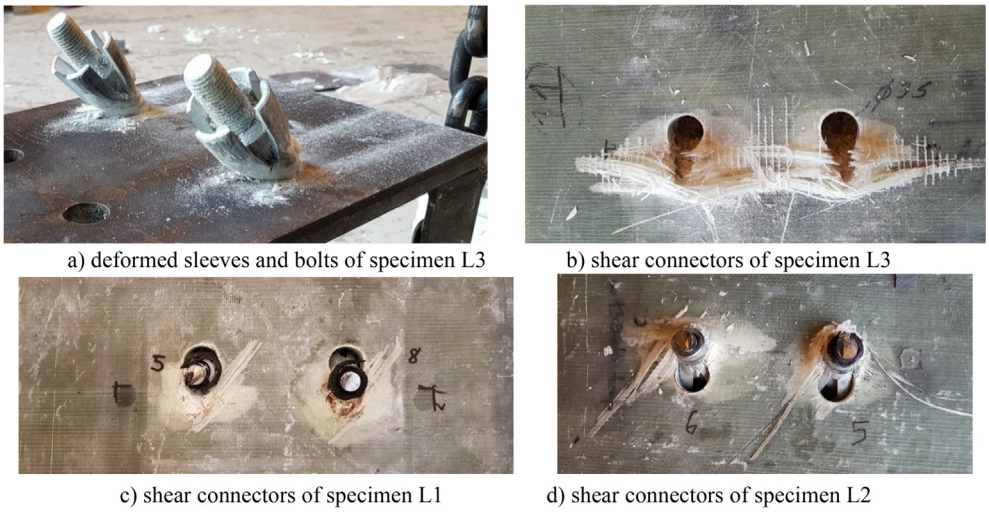

Fig. 5. Deformation of shear connectors and damages of FRP in Lindapter push-out specimens.

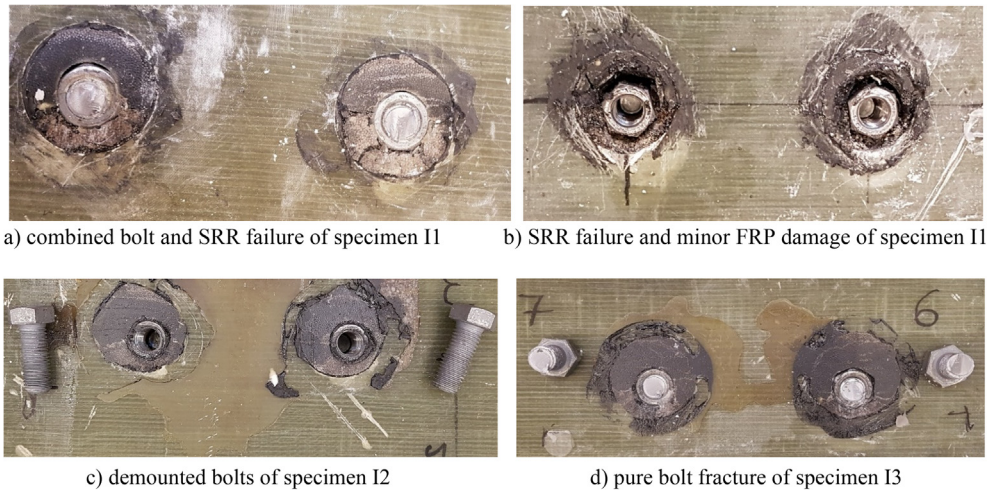

Fig. 6. Bolt shear failure and damages in injection piece of injected SRR push-out specimens.

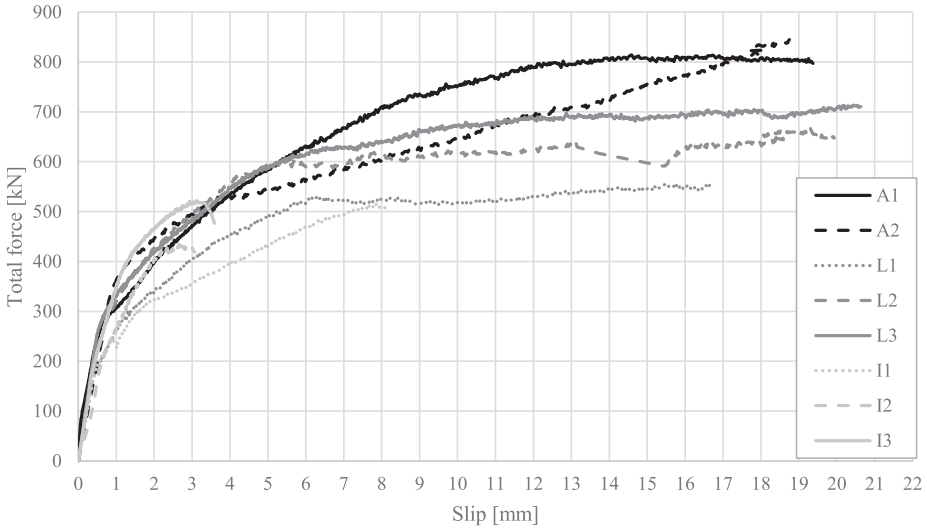

Fig. 7. Force-slip curves of Ajax, Lindapter and injected SRR connector specimens.

Table 2
Push-out test results.

Specimen (per connector)	F_{ult} [kN]	δ_{init} [mm]	δ_u [mm]	$\delta_{u,tot}$ [mm]	$k_{sc,in}$ [kN/mm]	k_{sc} [kN/mm]
A1	203.5	1.4	19.3	20.7	93	30
A2	211.2	4.8	18.5	23.3	99	20
L1	142.8	2.2	16.6	18.8	106	34
L2	168.0	3.1	19.8	22.9	111	45
L3	182.0	1.5	20.6	22.1	130	37
I1	128.9	0.6	8.0	8.6	104	29
I2	109.5	1.3	2.9	4.2	68	61
I3	130.5	1.4	3.5	4.9	122	85

40%, and slip to failure δ_u. Besides, the stiffness of the connection k_{sc}, is determined as secant stiffness at 0.7 F_{ult} (a.k.a. service load level) according to EC4 [12]. Also the initial stiffness $k_{sc,in}$ in the elastic range (up to 50kN) is given, being important for the level of hybrid interaction in a hybrid steel-FRP beam. The illustration of the definition of slip values used in this study is given in Fig. 8.

4.5. Comparison of connectors performance

The average shear resistances of Ajax and Lindapter connectors are 73% and 37% higher than the resistance of the iSRR connector (see Table 3), respectively. This is attributed to significantly larger shear area of the blind-bolted connectors provided by the sleeves, as shown in Table 1, although all connectors have M20 nominal diameter.

Similar initial connection stiffness $k_{sc,in}$, which is defined as slope of the elastic part of the load-slip curves shown in Fig. 7, was achieved by all three shear connectors, approximately 100 kN/mm. The initial connection stiffness of Lindapter slightly overpassed those of the other two, because during installation of the bolt the sleeve is firmly squeezed against the hole perimeter of the FRP plate.

The obtained initial slip δ_{init} values correlate with the initial bolt-to-hole clearances. Lindapter and Ajax bolts require oversized holes for bolt installation, as a consequence rather large initial slip (around 2–3 mm) was accumulated during cyclic loading. Up to 1 mm initial slip is obtained in case of the injected SRR connector. Small initial slip is important for proper and predictable behaviour of a steel-FRP hybrid beam because it provides hybrid interaction at low load levels.

Eurocode 4 [12] considers the shear connection as ductile if at least 6 mm slip occurs at 90% of the ultimate resistance after failure. For the Ajax and Lindapter shear connector types, high ductility was accomplished, approximately 20 mm slip, due to bearing failure in FRP. The absence of such failure mode in injected SRR specimens is favourable in terms of reusability of the FRP panel but comes at the cost of ductility of the shear connector resulting in an average characteristic slip of 3.2 mm at failure.

5. Description of the FE models

The 3D finite element (FE) models were built in Abaqus software package [23] version 6.14 and analysed with dynamic explicit solver to obtain quasi-static solution for the problem with multiple damage parameters of various materials and non-linear interfaces. The numerical analysis of the current study chiefly relies on the work of Pavlović [17] including his explorations to increase stable time step increment in explicit dynamic solver and strategy for implementation of damage material models for steel connectors. In this paper the approach is extended by implementing damage material models for FRP laminates and SRR injection piece.

5.1. Geometry, boundary conditions and analysis method

The geometry of the FE models of three connector types followed the design of the push-out specimens indicated in Fig. 2. Due to the double-symmetric geometry, loading and boundary conditions, only quarter of the push-out specimen is modelled to reduce computation time. The models comprise all components present in the push-out specimens: shear connector, HEB profile and the FRP panel, represented by plates of the facings, transverse webs and core, see Fig. 10. The connectors were modelled with their exact shapes, and all constituents i.e. bolts, washers, nuts, sleeves and the cone of Hollo-bolt represented as separate parts (Fig. 11). The aim is to model as much as possible complex interaction of the connectors' compo-

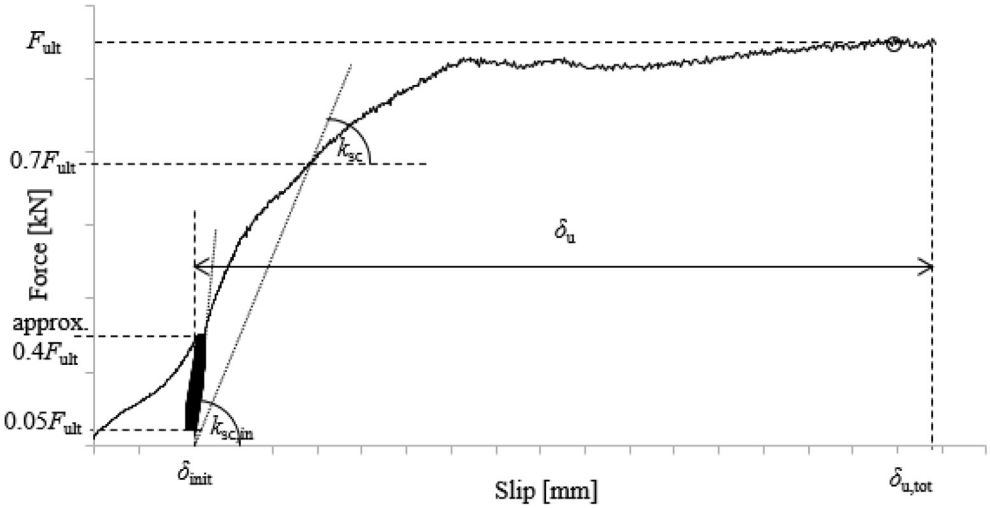

Fig. 8. Definition of slip values in this study.

Table 3
Averaged results of push-out tests.

Specimen	F_{ult} [kN]	δ_{init} [mm]	δ_u [mm]	$k_{sc,in}$ [kN/mm]
Ajax	207.4 (±5.4)	3.1	18.9 (±0.6)	96.0
Lindapter	164.3 (±19.9)	2.3	19.0 (±2.1)	115.8
Injected SRR connector	120.0* (±14.9)	1.1	3.2* (±0.4)	97.9

* Average of 'I2' and 'I3'. Due to the different failure mode of 'I1' it is excluded from the ultimate values.

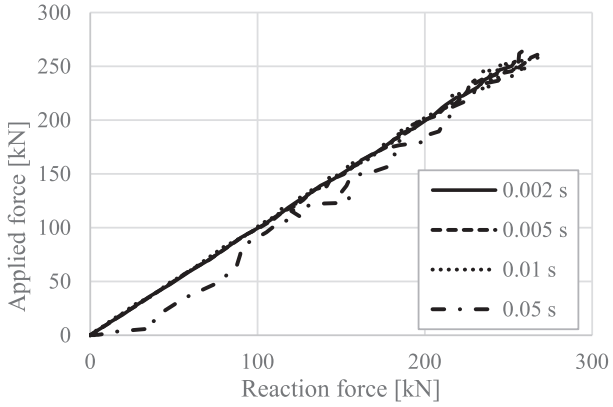

Fig. 9. Time step validation: compliance of the applied vs. reaction force in the push-out model.

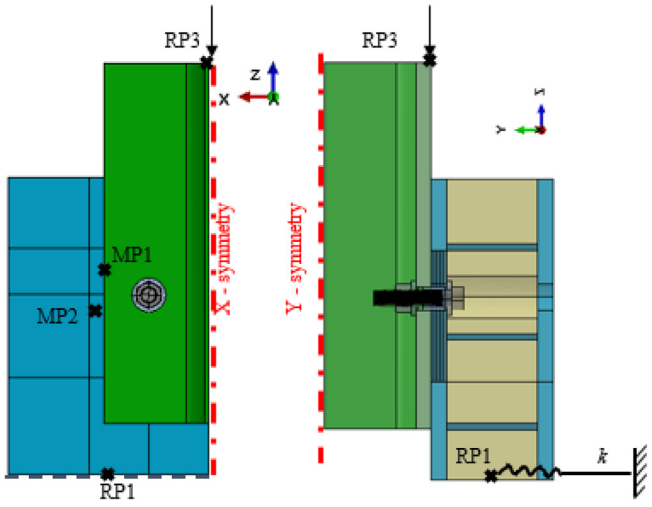

Fig. 10. Boundary conditions of FE models.

nents that might influence their local stiffness thus the load transfer and failure mode.

The nodes of the bottom of the FRP panel were coupled to a reference point (RP1) at the middle of the supporting surface. Fixed support boundary conditions were applied to RP1 reference point, apart from the lateral translation in *y* direction. In this direction the specimens in the push-out tests were laterally restrained by hollow steel profiles and threaded rods. Therefore, lateral support in the FE model was model with elastic springs corresponding to axial stiffness of the rods. The nodes on the upper end surface of the steel beam were coupled to a reference point (RP3). The load was applied as imposed vertical displacement on RP3 reference point with a smooth step amplitude curve, to minimize inertia effects in quasi-static explicit dynamic analysis [17].

The time period of the analysis was chosen similar to its real time period (e.g. 900 s for fracture loading), however, the quasi-static analysis was sped up by employing non-uniform, semi-automatic mass scaling in the explicit solver. The quasi-static response is valid if the inertia forces present in the dynamic system are negligible. The applicable value of desired time increment for integration of 0.005 s was found by minimising fluctuations on the graph of applied vs. reaction forces (see Fig. 9), and by limiting the ratio of kinetic energy to internal energy of the whole model (E_k/E_i) to 5% [23].

Slip of the connector is obtained with analogy to measurements by LVDTs in experiments (see Fig. 3), as the relative displacement between two points in the model, MP1 on steel flange and MP2 on the panel. Preloading of the bolts in the model (15 kN as snug tight in experiments) was applied through 'turn-of-nut method' - as is described in [17].

5.2. Finite element mesh

Linear, hexahedronal eight-noded solid elements, C3D8R with reduced integration were used for the steel beam and the sleeves of the blind bolted connectors. Linear tetrahedron elements, C3D4 were used for metallic parts with more complex geometry, namely the bolt, nut, washer, coupler, cone. Tetrahedron elements were as well used for the steel-reinforced resin (SRR) to cope with the complex inner geometry surrounding the embedded bolt and coupler.

The webs and facings of the FRP panel were modelled using four-noded SC8R continuum shell elements. Continuum shell elements were chosen over conventional shell elements to allow modelling of bearing of the connectors in relatively thick (20 mm) facing laminate and to allow for modelling of delamination between groups of plies in the vicinity of the connectors. The bottom facing of the FRP panel (the one in contact with steel beam) was divided into three regions, see Fig. 11a. In the middle area around the shear connector, where most of bearing and delamination damage is envisioned, 5 stacked continuum shell elements are used through the thickness to represent sub-laminates between which delamination is most likely – as is described in [21]. Sensitivity FE study showed that 1 mm element size is sufficiently small to model in plane stress concentrations governing the bearing failure and damage initiation and evolution around the connector. The rest of the FRP facings and webs were modelled with one continuum shell element through thickness and lay-up using laminated section. Relatively coarse mesh size of 10 mm was used in the periphery regions as stresses are limited to level of elastic behaviour. Tetrahedral elements of 1.2 mm size were used for the threaded parts of the connectors, according to calibration of the ductile damage material model [17]. These are the critical metallic components where damage can occur, therefore the mesh size was kept constant. Non-threaded parts of the steel connectors were modelled with hexahedron elements. As these parts exhibit only plastic deformation, no damage, the small mesh size of 2 mm was chosen only to ensure good modelling of contact interaction with the fine mesh of the threaded parts.

5.3. Interactions

Tie constraints, Cohesive Zone Model (CZM) and contact with friction were modelled using general contact algorithm of Abaqus/Explicit to simulate various interactions between the contacting parts of FRP laminates, steel plate, bolted connector, SRR and foam core of the

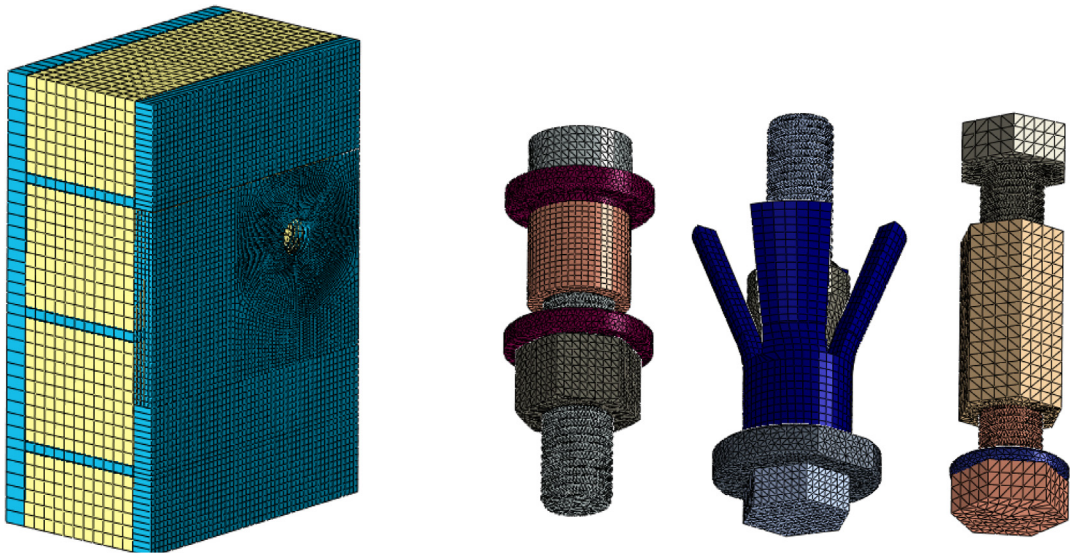

a) fine mesh of the bottom facing of FRP panel b) mesh of the shear connectors

Fig. 11. Details of the FE model of push-out test.

Table 4
Contact interaction between different parts of the FE models.

Part instance 1	Part instance 2	Contact type Blind bolted models	Contact type Injected model
FRP sub-laminate	FRP sub-laminate	CZM	CZM
FRP facings	FRP webs	tie	tie
FRP facings	PU core	tie	tie
Steel beam	FRP facing	μ = 0.2	μ = 0.2
Steel beam	Connectors	μ = 0.14	μ = 0.14
Steel beam	SRR	–	μ = 0.2
Bolts	FRP	μ = 0.2	μ = 0.2
Bolts	Coupler/Nut/Sleeve	μ = 0.14	μ = 0.14
Coupler	SRR	–	tie
Inner bolt	SRR	–	tie
FRP facings	SRR	–	μ = 0.2
PU core	SRR	–	tie

Table 5
Lay-up of the FRP laminates in the FRP panels.

Facings	$[0_4^\circ/45^\circ/-45^\circ/0^\circ/90^\circ][0_4^\circ/45^\circ/-45^\circ/0^\circ/90^\circ][0_4^\circ/45^\circ/-45^\circ/0^\circ/90^\circ]$ $[0_4^\circ/45^\circ/-45^\circ/0^\circ/90^\circ][0_4^\circ/45^\circ/-45^\circ/0^\circ/90^\circ/45^\circ/-45^\circ]$
Webs	$[45^\circ/-45^\circ/45^\circ/-45^\circ/0^\circ/90^\circ/45^\circ/-45^\circ/45^\circ/-45^\circ]$

FRP panel. Summary is given in Table 4. A friction coefficient of 0.14 was set between threads and nuts, while 0.2 was used for steel-FRP friction interaction according to [24,25]. Parameters of CZM used to model delamination inside facing laminate in the vicinity of the connector are shown in Table 8.

5.4. Material models

5.4.1. Material model of the FRP composite plates

The as produced stacking sequences shown in Table 5 were assigned to the continuum shell elements forming the facings and the webs of the FRP panel. The region in the vicinity of the connector hole is modelled with stacked sub-laminates indicated by intermittent parentheses in Table 5. The transversely isotropic elastic material properties of the UD plies constituting the laminated of facings and the webs are presented in Table 6. The values are obtained from standard material tests by the panel producer.

Hashin damage material model was applied for the progressive damage analysis of in-plane ply failure [23]. The material is considered as linear elastic until the failure criteria is reached, followed by linear softening of the stress–strain curve, based on the given value of fracture energy. In the Hashin damage model four failure modes are distinguished: fibre tension, fibre compression, matrix tension and matrix compression failure. The reference [11] shows a good example of successful usage of Hashin model in ABAQUS to model the damage of FRP used in a pultruded FRP deck.

The damage material parameters in the analysed push-out models – the 6 strength values and 4 fracture energies of the UD ply, shown in Table 7, were calibrated as shown in the accompanying paper [21]. CZM parameters used to model delamination between sub-plies around the connectors are shown in Table 8 as calibrated in [21].

5.4.2. Steel material models

Plasticity and ductile damage models for metals in Abaqus [23] were used in this study, as indicated in Table 9. Elastic constants (E = 210 GPa, and ν = 0.3) and nominal yield and ultimate stresses in combination with isotropic hardening were used for steel profile (S355, f_y = 355 MPa; f_u = 510 MPa) and sleeve of the Hollo-Bolt

Table 6
Linear-elastic material properties of UD plies.

Material name	Elastic constants [GPa]	Poisson's ratio	Density [kg/m^3]
Elastic FRP UD ply V_f = 54% - in facings	E_1 = 31.450, E_2 = E_3 = 8.459, G_{12} = G_{13} = 4.838, G_{23} = 3.021	ν_{12} = ν_{13} = 0.272, ν_{23} = 0.4	1873
Elastic FRP UD ply V_f = 28% - in webs	E_1 = 21.170, E_2 = E_3 = 5.690, G_{12} = G_{13} = 3.260, G_{23} = 2.032	ν_{12} = ν_{13} = 0.308, ν_{23} = 0.4	1539

Table 7
Failure and damage material parameters of UD ply.

	Longitudinal tensile	Longitudinal compression	Transverse tensile	Transverse compression	Longitudinal shear	Transverse shear
Strength [MPa]	865	700	36	131	87	75
Fracture energy [N/mm]	92	80	0.2774	0.7979	–	–

Table 8
Parameters of cohesive surface interaction property.

	Normal – mode I	Shear – mode II and III
Contact strength [MPa]	21	30
Fracture energy [N/mm]	0.9	4.0

Table 9
Overview of material modelling approach for various steel parts in FE model.

Part	Plasticity curve	Ductile damage	Shear damage
HEB260 – steel profile	S355	included	–
Bolts – all connectors	8.8	included	included
Nuts – all connectors	8.8	included	included
Washers – all connectors	10.9	–	–
Sleeve – Ajax con.	10.9	–	–
Sleeve – Lindapter con.	S275	–	–
Coupler – Injected SRR con.	10.9	included	included

(S275; f_y = 275 MPa and f_u = 390 MPa). The material and damage model of bolts grade 8.8 and 10.9 were adopted from the research of Pavlović [17], where the ductile and the shear damage parameters were calibrated based on standard tensile coupon tests and bolt shear tests. The parameters for shear damage of the bolt are the most relevant and were defined by equivalent plastic strain at the onset of damage of $\bar{\varepsilon}_s^{pl} = 0.08$, equivalent plastic displacement at failure $\bar{u}_{f,s}^{pl} = 0.3mm$ and exponential law parameter of 0.7 as in [17].

5.4.3. Material model of SRR

SRR exhibits different behaviour in compression and tension. In many aspects SRR material resembles material behaviour of concrete, except having more ductility in tension. As such, the Concrete Damage Plasticity (CDP) model integrated in Abaqus [23] is utilised for modelling the SRR behaviour, able to model local confinement effect in the zone around connector as shown by [17]. Mean values of young's modulus, compressive and tensile strength, E = 9.3 GPa, f_c = 74.3 MPa, and f_t = 10.1 MPa, respectively, were used in CDP as determined on cylinders and split tests shown in [26]. The initial part of the compressive stress–strain curve for SRR was obtained by matching it to test result of compressive cylinder (see Fig. 12a). The softening part of the stress–strain curve in compression follows the shape recommended by [27] to idealise the uniaxial behaviour of concrete in compression. In tension, the material is assumed to be linear elastic until full tensile strength followed by cracks opening represented by sinusoidal softening until 0.05 f_t at 0.02 cracking strain (Fig. 12b). Relatively low residual tensile strength is used to resolve issues of convergence of numerical solution. The CDP assumes non-associated potential plastic flow. In CDP, Drucker-Prager hyperbolic function is used as flow potential. The flow potential eccentricity was set to ε = 0.1 according to the recommendation of [23], the ratio of biaxial/uniaxial compressive strength was assumed as $\sigma_{bo}/\ \sigma_{co}$ = 1.2. The other plasticity parameters were calculated according to [28]: the dilation angle was evaluated as ψ = 50.5°, and the parameter K = 0.78 were determined iteratively to match the experiment results. Separate damage laws for compression and tension were defined according to the procedure shown in [17].

6. Validation of experimental vs. FEA results

Numerical models could predict well the load-slip behaviour of the push-out experiments, see Fig. 13, as well as capture all failure modes as shown in Fig. 14 and Fig. 15.

Considerable bearing, and delamination damage together with significant bolt deformation was detected in case of the blind bolted shear connectors both in FEA and in experiments. FE model of the injected SRR connector realistically reproduces the bolt shear failure. A known limitation [21] due to severe element distortion, resulted in early termination of the analysis before reaching extremely large slip of 20 mm found in Ajax and Lindapter experiments. However, modelling the failure with such deep bearing penetration, up to 11 mm is considered as an achievement of the presented FEA. As the very late nonlinear stage of the connectors is reached, the FEA results are considered appropriate to investigate the elastic and failure behaviour of blind bolted connectors.

The shear resistance of the injected SRR connector predicted by FEA contrasted to experimental result and the comparison of force values of the Ajax and Lindapter FE models at the slip corresponding to the end of numerical analysis to the experimental results are given in Table 10. All results are within 10% accuracy, which is acceptable considering the complexity of interaction and sensitivity of damage parameters of the material models.

The global damage index DAMAGESHR, which combines different fibre and matrix damage modes is shown for the illustration of in-plane ply damage in Fig. 15. The contour plots of damage index of cohesive

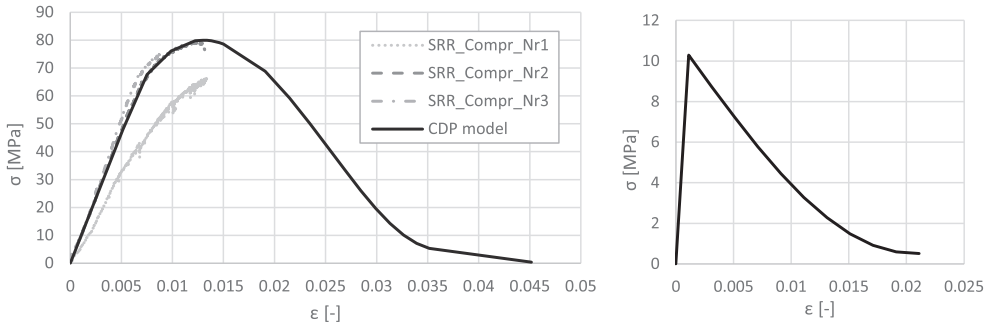

Fig. 12. Stress–strain curves of SRR.

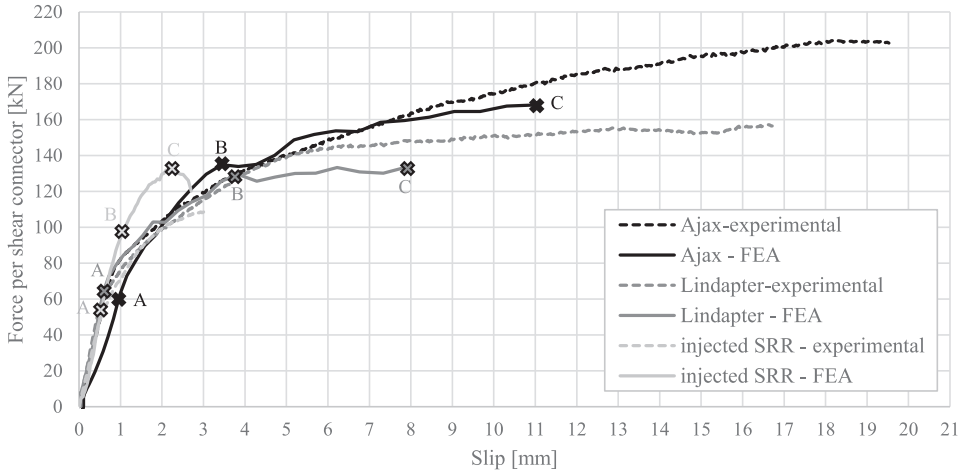

Fig. 13. Experimental and numerical force-slip curves.

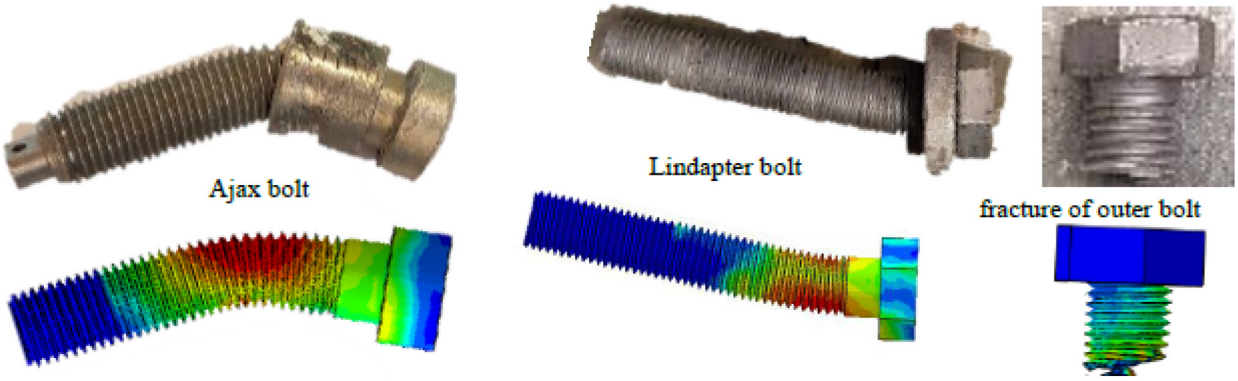

Fig. 14. Bolt deformations at the end of experiment vs end of analysis (point C).

surface property CSDMG, is given to show good match between the delamination damage found in FEA and experiments.

7. Discussion of FEA results

7.1. Failure mechanism

Three representative load levels are marked on the force-slip curves of Fig. 13: A is at the onset of nonlinearity, B is midway between A, and the end of the analysis/maximum load level C. The load-slip curves of Fig. 13 show similar tendency for the two blind bolted connectors: there is a considerable loss of stiffness at load level B, while for the injected SRR connector, the change in slope of the curve after point B is less apparent. The reason for the difference can be explained by following the damage progression and deformation of the three shear connectors throughout the analysis as are displayed in Fig. 16. The notations A, B and C corresponds to the 3 load levels.

At the end of elastic connector behaviour, all bolts are completely straight, the stresses in the bolts are within the elastic range (Fig. 16A). At load level B, the blind bolted connectors slightly rotate, the Ajax bolt also starts to bend and due to the inclination of the bolts, the FRP plate around the delaminates around the hole (Fig. 16B). The rotation and bending of the bolts, together with the laminate failure generate a rapid loss of connection stiffness. In contrast to the blind bolts, in case of injected SRR connector, the yield strain due to shear is first reached in the middle of the cross-section of the bolt and spreads through the entire cross section without noticeable bolt bending or rotation, thus the connection stiffness does not change significantly.

At the end of the analysis (point C), the blind bolted connectors are significantly rotated, the Ajax bolt also exhibits severe bending deformation. At this load level the shear damage initiation criteria is met at the weakest cross-sections (Fig. 16C): above the sleeve in the Ajax bolt, between the washer and the expandable sleeve in the Lindapter bolt and in the entire cross-section of the injected SRR connector, leading to bolt fracture (Fig. 14). The bolt rotation of the Ajax and Lindapter connectors creates out-of-plane stresses acting on the laminate, resulting in further spread of delamination damage (Fig. 16C).

Similar damage progression analysis is given in Fig. 17 for the SRR injection piece. Two possible failure modes can be associated with the SRR injection piece: crushing failure of SRR in front of the mechanical shear connector, and tensile cracking behind the coupler due to local bending of the SRR injection piece. The development of compressive and tensile damage variables, representing these two potential failure modes, are shown in Fig. 17 with respect to load levels A, B and C. In the early stages of the loading, only tensile damage appears in the injection piece. The crack initiates from the junction of enlargement ring and the back surface of the coupler (Fig. 17A, B). Prior to failure, the inclined crack almost reaches the top corner of the coupler, which would result in an additional, sudden slip of the connection. Compressive damage of SRR occurs only at the highest load level as crushing

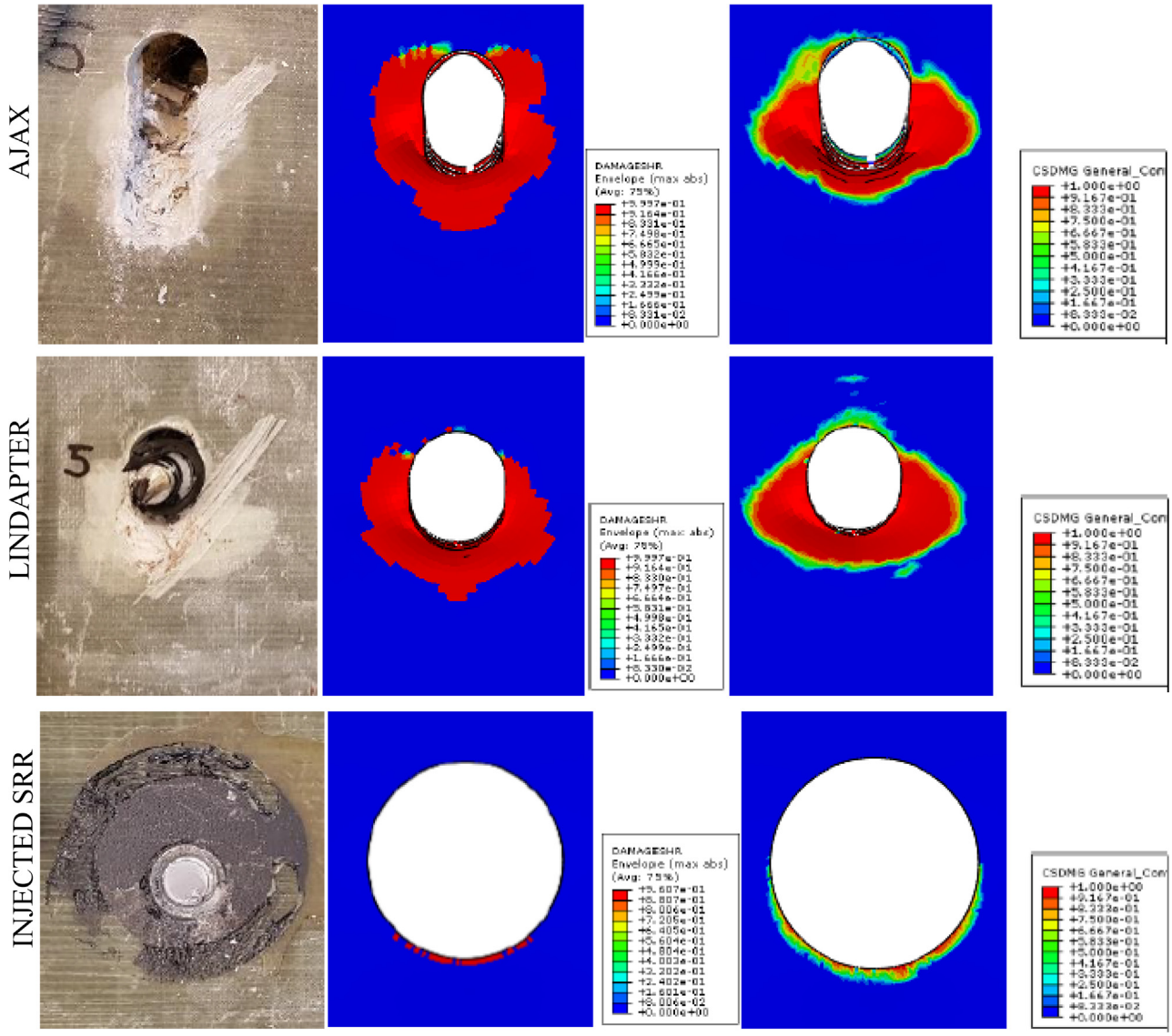

Fig. 15. FRP bearing failure: experiments vs. FEA (shear damage index, damage of contact domain) at load level C.

Table 10
Experimental and numerical results of push-out tests.

Shear connector	Force at the slip value of point C (F_C) or shear resistance (F_{ult})		
	Experimental [kN]	Numerical [kN]	Difference [%]
Ajax	$F_{C,Exp}$ = 180.2	$F_{C,FEA}$ = 168.1	6.7
Lindapter	$F_{C,Exp}$ = 147.8	$F_{C,FEA}$ = 139.4	5.7
Injected SRR	$F_{ult,Exp}$ = 120.0	$F_{ult,FEA}$ = 132.0	10.0

inside the hole in bottom facing of the FRP panel (Fig. 17C). Overall, the contribution of SRR damages to the final failure mode of injected SRR connector is negligible.

7.2. Deformation analysis

Both the push-out test results (section 4) and the damage plots of section 7.1 have already shown, that bearing failure of the laminate, loose rotation and plastic deformation of the bolts are the main contributors to the very large slip capacity of the blind bolted shear connectors. On contrary, high stiffness and the limited slip capacity of the injected SRR connector is attributed to the gapless design and execution of the connection and inherently brittle failure mode of the bolt. These observations are quantified by analysing the development of the total relative displacement (slip) decomposed to connection components. Results are shown in Fig. 18. The ovalisation of the hole, namely the bearing failure of the laminate contributes the most, with 75%, to the total slip of the blind bolted Ajax and Lindapter connectors. The second most significant component is the deformation of the bolt, approximately 20%. On the other hand, elastic–plastic shear/bending deformation of the bolt (34%) and mostly elastic deformation of the injected piece (26%) are the two dominant contributors to relative displacement in case of the injected SRR connector. The marginal 8% contribution of hole ovalisation of the bottom facing shows the design objective of iSRR connectors to limit the bearing stresses/damage is accomplished.

7.3. Shear load transfer analysis

There is a significant difference in the load-slip behaviour of the analysed connectors, see Fig. 13, which is the consequence of different shear load transfer mechanisms. Load-slip curve of the Ajax shear con-

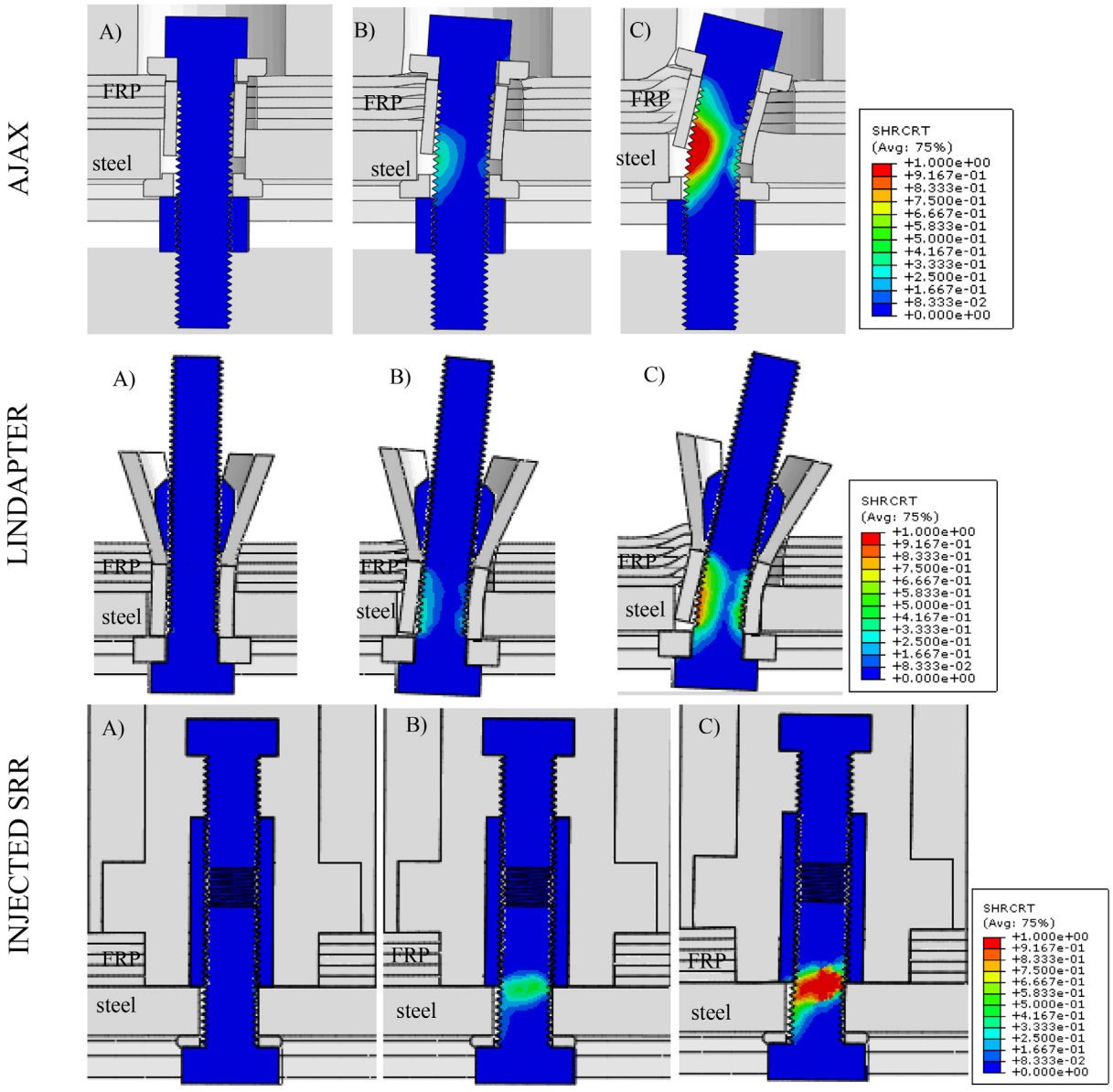

Fig. 16. Shear damage index of steel components and deformation figures at the 3 representative load levels.

nector exhibits a sort of hardening behaviour, meaning that the load continuously increases with increasing slip. On the contrary, the Lindapter shear connector shows a characteristic plateau in the load-slip curve between points B and C. The reason for the difference between the two blind bolted connectors lies in the catenary effects in the bolts. As it can be seen in Fig. 16B and C, Ajax and Lindapter connectors undergo severe rotation at load levels surpassing the linear behaviour of the connection. Because both bolted connectors are anchored inside the FRP panel, the shear load applied to the connection results in catenary effects in the rotated bolts, leading to a rise of axial force, as the shear load is increased. Axial force in the Ajax bolts reaches value of $N_{\text{bolt}} = 123.42$ kN which is double, compared to the axial force in Lindapter bolt ($N_{\text{bolt}} = 59.31$kN) at similar load level, as can be seen in Fig. 19 obtained from the FEA results. This difference is attributed to the dissimilar fixation principles of the two types of blind bolts inside the FRP panel. In case of the Ajax connector, the inner head and the washer provides better anchorage to the FRP plate, compared to the expandable sleeve of the Lindapter shear connector which fails to prevent the rotation of the end of the bolt (see Fig. 16C). As a consequence, the Lindapter connector partially pulls out from the FRP plate and thus lower axial force is generated.

Internal force components contributing to the shear load transfer of the connection F_{tot} are indicated in Fig. 19b on example of Ajax connector. Same principle is used for other connectors. The basic shear resistance is provided by the shear force in the bolt shank and the sleeve $V_{\text{b\&sl}}$. The catenary force F_{cat} is the vertical component of the axial force in the bolt F_x rotated by the angle α. The axial tension force in the connector F_x results in compressive contact stresses at the steel-FRP interface which in turn induces additional friction resistance F_{fric}. Hence:

$$F_{tot} = V_{b\&sl} + F_{cat} + F_{frict} \tag{1}$$

The internal force components are obtained from FEA results by integrating internal stresses in the bolts, analysing rotation of the bolt and integrating contact shear stresses at the steel-FRP interface. The development of all internal force components is given in Fig. 20a on example of Ajax bolt. In Fig. 20b comparison is given for the relative contribution of all internal force components for different connectors

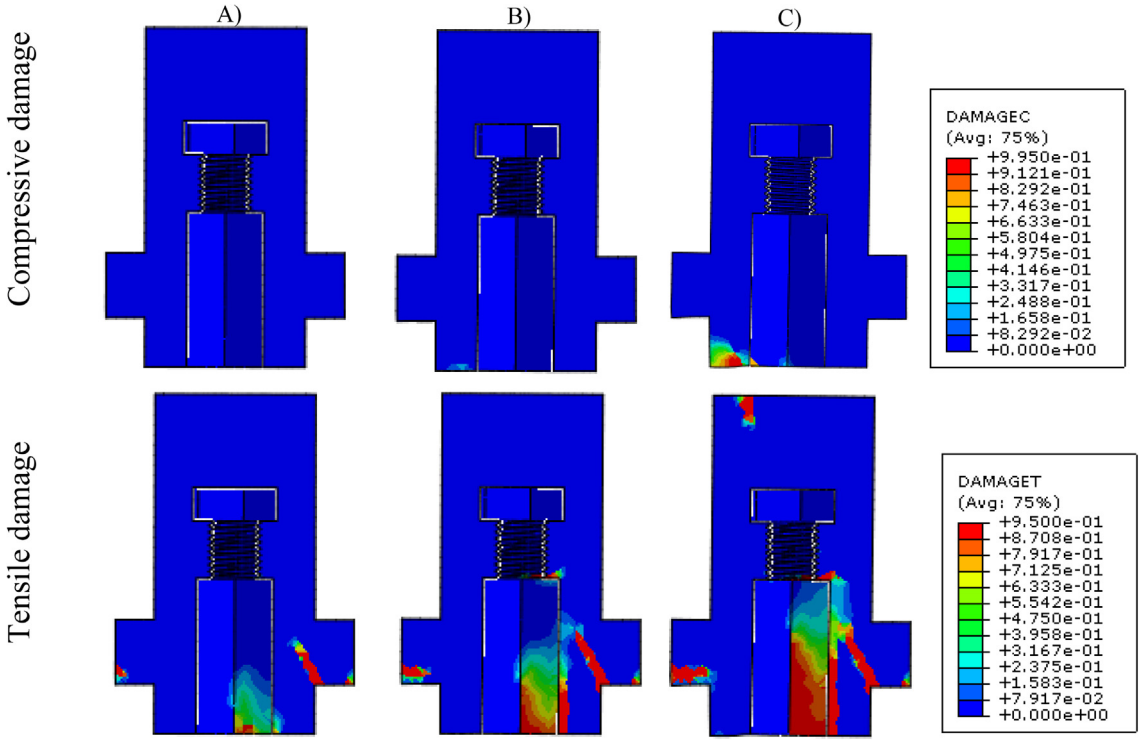

Fig. 17. Compressive and tensile damage of SRR at the 3 representative load levels.

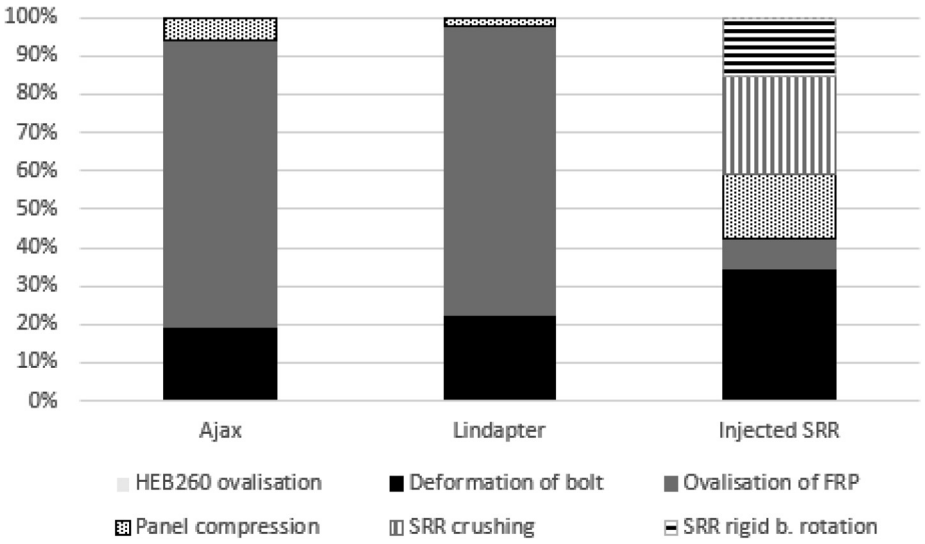

Fig. 18. Decomposition of slip displacement in the FE models.

at the final loading stages (load level C). Catenary forces and friction forces in Ajax connector contribute by approx. 20% and 10% respectively, which explains the high shear resistance with a sort of hardening behaviour. Friction forces in case of Lindapter connection contribute much less because the bolt pulls-out of the hole of the FRP plate, failing to develop large contact stresses at the steel-FRP interface, see Fig. 16C. Severe rotation of the Lindapter connection, on the other hand, results in a significant 15% contribution of the catenary forces in the shear load transfer.

Even though at the final loading stage similar axial force is developed in case of injected SRR connector as in the Lindapter connector (see Fig. 19a), the absence of bolt rotation impeded by the marginal crushing damage of the SRR injected piece, results in no significant catenary forces, see Fig. 20b. However, given the fact that the connector is well clamped inside the FRP panel and there is a substantial axial force at the final stage of loading, contact stresses develop at steel-FRP interface leading to 5–10% contribution of friction forces in the shear load transfer.

8. Conclusions

In this study, push-out tests were conducted to investigate the structural behaviour of demountable shear connectors connecting web-core FRP deck panels to steel girder for steel-FRP composite structures. The parameter varied in the experiments was type of the shear connector. Shear behaviour of two blind bolted shear connectors (Ajax and Lindapter) with nominal diameter of 20 mm and a novel injected SRR connectors developed at TU Delft were compared based on the

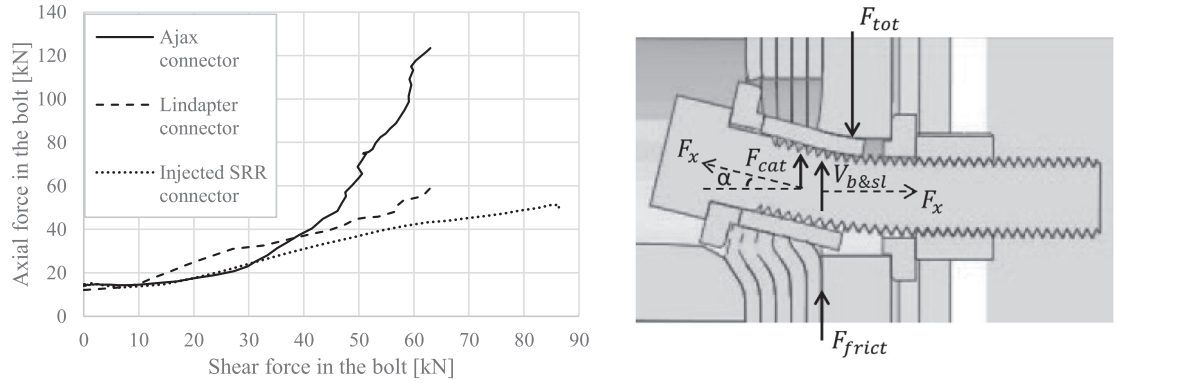

a) development of axial forces b) force components in connectors (example of Ajax bolt)

Fig. 19. Development of axial force in the bolts due to catenary effects.

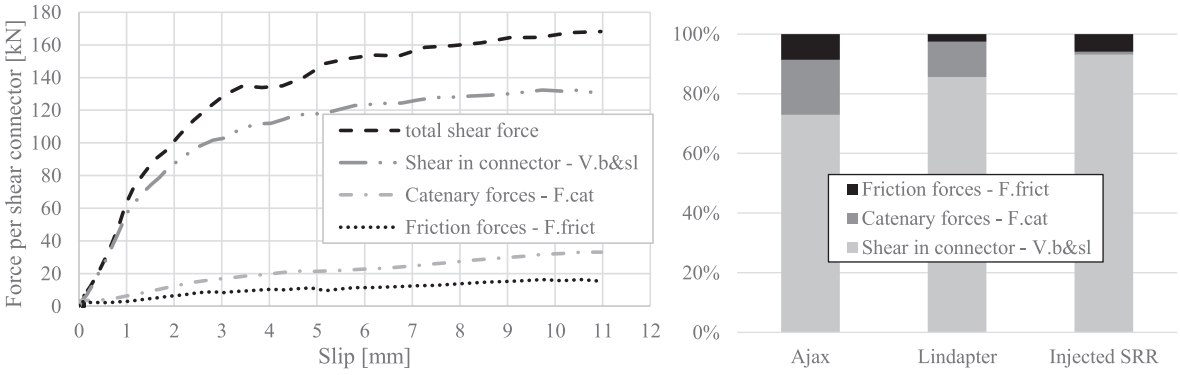

a) development of internal force components (example Ajax connector) b) contribution of internal forces in shear load transfer

Fig. 20. Decomposition of internal forces in the shear load transfer.

quantified shear resistance, connection stiffness and ultimate slip values obtained from the experiments. Failure mechanisms of three types of shear connectors are also thoroughly explained and compared through results of detailed 3D non-linear FE models. The FE models are validated by good agreement to load-slip behaviour in push-out experiments and capturing exact failure modes. The following conclusions are drawn:

- The shear resistance of approximately 200 kN and 120 kN were found for blind-bolted and injected SRR connectors, respectively. The initial shear connector stiffness of all three examined shear connectors in FRP deck is around 100 kN/mm, which is comparable to that of bolted connections in steel–concrete composite structures.
- All specimens with blind bolted shear connectors (Ajax and Lindapter) failed by excessive local crushing (bearing damage) of the bottom facing of FRP panel in combination with rotation and plastic bending of the bolts. These failure modes favour ductility of the connection: e.g. according to the FE analysis, ovalisation of the hole (as a consequence of bearing damage) contributed with 75% to the remarkable, up to 20 mm, slip capacity. Although the Lindapter connector exhibited remarkable bolt deformation, the bolt has not ultimately pulled out from the bolt hole during the push-out experiments, thus ensuring the connection integrity.
- Conversely, bolt shear failure characterizes the push-out behaviour of injected SRR specimens, where bearing deformation contributed only 8% to the total slip, leaving no damage in the FRP, thus providing chance for reuse of the panel in the second life cycle. This comes at the cost of lower slip capacity, with average 3.2 mm ultimate slip. Although some crushing of the SRR occurs in the zone of bottom facing of the FRP panel according to the FE analysis, the integrity of the SRR injection piece remains intact.
- The detailed FE analysis revealed, that both blind bolted connectors, Ajax and Lindapter, show increase of shear resistance in the non-linear range of the load-slip curve, i.e. hardening behaviour, due to catenary effects of the connectors. The axial force that develops due to the rotation of the bolt contributes in the shear load transfer by 10–20%. In injected SRR connectors the catenary effects are negligible.
- The FE analysis demonstrated that Ajax connectors show better hardening in the post-elastic phase of the shear behaviour resulting in 25% larger shear resistance vs. Lindapter connectors. This is due to presence of the foldable washer inside the FRP panel which provides “good grip” to the bottom facing of FRP panel and therefore leads to larger axial force: 120 kN vs. 60 kN developed in the Ajax vs. Lindapter bolt shanks. The large axial force of Ajax connector results in a 10% contribution of the friction forces at the steel-FRP interface to the total shear load transfer.

CRediT authorship contribution statement

Fruzsina Csillag: Methodology, Validation, Data curation, Writing - original draft, Visualization. **Marko Pavlović:** Supervision, Methodology, Project administration, Funding acquisition, Writing - review & editing.

Declaration of Competing Interest

The authors declare that they have no known competing financial interests or personal relationships that could have appeared to influence the work reported in this paper.

Acknowledgements

The authors are very grateful to all supporters of their research: to FiberCore Europe b.v. for supplying FRP deck panels, to Ajax Fasteners for providing connector specimens and to Bouwen met Staal organization for supporting the lab work.

The raw data required to reproduce these findings are available to download from Csillag, Fruzsina; Pavlovic, Marko (2019), "Data for: Push-out behaviour of demountable shear connectors for steel-FRP hybrid beams – Part 1: Experiments", Mendeley Data, V2, doi: 10.17632/2427x8rb4f.2.

References

[1] Righman J, Barth K, Davalos J. Development of an efficient connector system for fiber reinforced polymer bridge decks to steel girders. Compos Constr 2004;8:279–88.
[2] Alampalli S, Kunin J. Rehabilitation and field testing of an FRP bridge deck on a truss bridge. Compos Struct 2002;57:373–5.
[3] Solomon G, Godwin G. Expanded use of Composite Deck Projects in USA. Struct Eng Int 2002;2:102–4.
[4] Knippers J, Gabler M. New design concepts for advanced composite bridges–The Friedberg Bridge in Germany. In: IABSE Symposium Report: International Association for Bridge and Structural Engineering; 2006. p. 16-23.
[5] Moon FL, Eckel DA, Gillespie JW. Shear stud connections for the development of composite action between steel girders and fiber-reinforced polymer bridge decks. J Struct Eng 2002;128:762–70.
[6] Chou C-C, Chen Y. Push-off strength of steel girder to fiber-reinforced polymer deck connections. J Constr Steel Res 2013;81:138–48.
[7] Satasivam S, Bai Yu. Mechanical performance of modular FRP-steel composite beams for building construction. Mater Struct 2016;49:4113–29.
[8] Gürtler H. Composite action of FRP bridge decks adhesively bonded to steel main girders. Lausanne EPFL 2004.
[9] Park K-T, Kim S-H, Lee Y-H, Hwang Y-K. Degree of composite action verification of bolted GFRP bridge deck-to-girder connection system. Compos Struct 2006;72:393–400.
[10] Satasivam S, Bai Y. Mechanical performance of bolted modular GFRP composite sandwich structures using standard and blind bolts. Compos Struct 2014;117:59–70.
[11] Xin H, Mosallam A, Liu Y, Wang C, Zhang Y. Analytical and experimental evaluation of flexural behavior of FRP pultruded composite profiles for bridge deck structural design. Constr Build Mater 2017;150:123–49.
[12] EN1994-1-1. Eurocode 4 - Design of composite steel and concrete sturctures. Part 1-1: General rules and rules for buildings. Brussels, Belgium: European Committee for Standardization (CEN); 2010.
[13] fasteners A. https://site.irasvens.com/?page_id=4705.
[14] Hollo-Bolt LTH. www.lindapter.com.
[15] Wijesiri Pathirana S, Uy B, Mirza O, Zhu X. Flexural behaviour of composite steel–concrete beams utilising blind bolt shear connectors. Eng Struct 2016;114:181–94.
[16] Mirza O, Uy B, Patel N. Behaviour and strength of shear connectors utilising blind bolting. In: Steel and Composite Structures: Proceedings of the 4th International Conference on Steel and Composite Structures, 21-23 July 2010, Sydney, Australia; 2010. p. 791-6.
[17] Pavlović M. Resistance of bolted shear connectors in prefabricated steel-concrete composite decks. Belgrade: University of Belgrade; 2013.
[18] Nijgh MP. New Materials for Injected Bolted Connections - A Feasibility Study for Demountable Connections. Delft University of Technology; 2017.
[19] Nijgh MP, Xin H, Veljkovic M. Non-linear hybrid homogenization method for steel-reinforced resin. Constr Build Mater 2018;182:324–33.
[20] Europe F. https://www.fibercore-europe.com/en/sustainable-bridges/infracore-technology/.
[21] Csillag F, Pavlovic, M., van der Meer, F. Progressive Damage Analysis of pin bearing failure in GFRP using continuum shell FE modelling approach. In: ACIC (Advanced Composites in Construction). Birmingham, UK; 2019.
[22] ASTM D 5961-05: Standard test method for bearing response of polymer matrix composite laminates. West Conshohocken, PA, USA: ASTM International; 2005.
[23] Abaqus-Inc. Abaqus User Manual, Version 6.14. In: Providence R, editor. USA: Dassault Systémes Simulia Corp.; 2014.
[24] Du A, Liu Y, Xin H, Zuo Y. Progressive damage analysis of PFRP double-lap bolted joints using explicit finite element method. Compos Struct 2016;152:860–9.
[25] Turvey GJ. 3 - Bolted joints in pultruded glass fibre reinforced polymer (GFRP) composites. In: Camanho P, Tong L, editors. Composite Joints and Connections: Woodhead Publishing; 2011. p. 77-111.
[26] Csillag F. Demountable deck-to-girder connection of FRP-steel hybrid bridges. Delft: Delft Technical University; 2018.
[27] Pavlović M, Marković Z, Veljković M, Buđevac D. Bolted shear connectors vs. headed studs behaviour in push-out tests. J Constr Steel Res 2013;88:134–49.
[28] Haohui Xin MN, Milan Veljkovic. Computational homogenization simulation on steel reinforced resin used in the injected bolted connections. Compos Struct 2019;210:942-57.